ISSN (Print) 1226-1750
ISSN (Online) 2233-6656
Journal of Magnetics 18(4), 432-442 (2013) http://dx.doi.org/10.4283/JMAG.2013.18.4.432

Gimballing Flywheel and its Novel Reluctance Force-type Magnetic Bearing with Low Eddy Loss and Slight Tilting Torque

Jiqiang Tang*, Chun'e Wang, and Biao Xiang

School of Instrument Science and Opto-electronics Engineering, Beihang University, Beijing 100191, China

(Received 15 February 2013, Received in final form 17 September 2013, Accepted 24 September 2013)

For magnetically suspended flywheel (MSFW) with gimballing capability, demerits of Lorentz force-type magnetic bearings and common reluctance force-type magnetic bearings are analyzed, a novel reluctance force-type magnetic bearing (RFMB) including radial and axial magnetic bearing units with 4 separate biased permanent magnets and two conical stators is presented. By equivalent magnetic circuits' method, its magnetic properties are analyzed. To reduce the eddy loss, it was designed as radial poles with shoes and its rotor made of Iron-based amorphousness. Although the uniformity of magnetic flux density in the conical air gap determines mainly the additional tilting torque, the maximum additional tilting torques is 0.05Nm and the rotor tilting has no influence on its forces when the rotor tilts or the maximum changes does not exceed 14% when the rotor drifts and tilts simultaneously. The MSFW with this RFMB can meet the maneuvering requirement of spacecraft theoretically.

Keywords : reluctance force-type magnetic bearing (RFMB), gimballing flywheel, tilting, additional torque

1. Introduction

Flywheel is an inertial actuator in a spacecraft attitude control system to generate suitable attitude control torques for correcting spacecraft attitude deviation or adjusting to an assigned attitude [1-4]. The attitude control torque generated by changing the rotational speed of rotor of flywheel has high torque precision but cannot meet the maneuvering requirement fully for some space applications [5, 6]. Compared with conventional ball bearing flywheels, the magnetically suspended flywheel (MSFW) has advantages of no friction, free lubrication, low losses, and theoretically unlimited lifetime [7-11]. As for the 5 degree-of-freedom (DOF) MSFW, the rotor can be actively controlled in all 5 DOFs, so the momentum vector of the flywheel can be tilted actively with respect to the spacecraft body (named as 'vernier gimballing') to generate control moment in the other two directions [11, 12]. For these space applications of a MSFW with gimballing capability, its structure has been studied in [11] and [13]. U. Bichler [14] and K. Yabuuchi [15] proposed an attitude control scheme for large angle attitude maneuvers, Y. Kim [13] researched the interaction dynamics between a satellite and on board gimballing MSFWs. Be superior to other attitude actuators, this kinds of MSFW has promise to fulfill the requirements of both precision and maneuvers and it is possible to decrease the number of the needed flywheels to control the attitude of spacecraft.

With respect to the MSFW with gimballing capability, these magnetic bearings can be divided into Lorentz force-type magnetic bearings and reluctance force-type magnetic bearings according to the physical cause of the generation of the force. For the Lorentz force-type magnetic bearings, the force per unit length of conductor generated by the interaction of the current $\vec{i}$ and the magnetic flux density $\vec{B}$ is orthogonal to the flux lines, independent of the air gap and linearly dependent on the current [14-16]. For the reluctance force-type magnetic bearings, the magnetic force per unit area is given by B^2/μ_0, where B is the magnetic flux density in the air gap and μ_0 is the vacuum permeability. J.C. Fang, J.Q. Tang *et al.* [17-19] paid attention to study a permanent magnet biased axial hybrid magnetic bearing, which is one kind of reluctance force-type magnetic bearings. However, due to the magnetic flux being inversely proportional to the gap length, the tilting angle of rotor is very small and can't beyond 0.1° generally, the generated control moment is only about 0.1Nms, which is too small for MSFW with gimballing ability.

*Corresponding author: Tel: +86-01082316813
Fax: +86-01082317396, e-mail: tjq_72@163.com

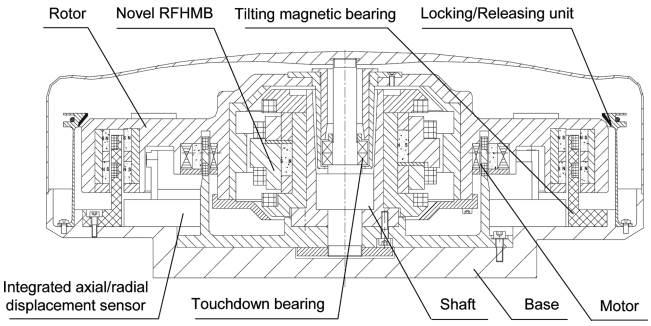

Fig. 1. Momentum flywheel with gimballing capability.

In one MSFW with gimballing capability as shown in Fig. 1, there are one rotor, one presented novel reluctance force-type magnetic bearing (RFMB), one tilting magnetic bearing, one integrated axial/radial displacement sensor, one motor, two touchdown bearings, one shaft and one base. The novel RFMB located in the center of the flywheel is used to control both axial and radial translation of rotor. The tilting magnetic bearing arranged in the outer rim of the rotor is used to make the rotor rotate around x or y-axis to generate large control moment. The displacements and tilting angles of rotor are measured by the displacement sensors. Two touchdown bearings are used to support the rotor when the magnetic bearings are turned off or in case of failure. Due to the novelty and specialty of RFMB, the rotor of MSFW with gimballing capability can be tilted beyond 1° and its outputting control moment is up to 3.3 Nm, both of them are far larger than that of existing same kind MSFW, then the MSFW with gimballing capability can meet the maneuvering requirement of spacecraft fully.

For this MSFW installed in satellite, environment tests such as acceleration test and vacuum thermal cycle test are very important. When it is under high frequency acceleration, the rotor is locked by the locking/releasing unit as shown in Fig. 1. In other conditions, the rotor is released from the locking/releasing unit and keeps free.

This paper emphasizes on the analysis of additional torques of different gimballing flywheel with existing RFMBs and how to design a novel RFMB with low eddy loss and slight tilting torque. The special structure of RFMB is our original novelty and how to analyze its suspension properties are our main contributions. In order to decouple the suspension forces not only between X and Y dimension but also between radial direction and axial direction, suspension properties in radial and axial directions, torque characteristics, coupling properties when rotor is shifted or tilted are researched deeply by theoretical analysis and finite element method.

2. Additional Torques of Gimballing Flywheel with Existing RFMB

For the MSFW with gimballing capability, the reluctance force-type magnetic bearings used in it can be classified into two types generally according to their arrangement and structure. The arrangement and structure of 1st type MSFW and the generation of additional tilting torque are shown in Fig. 2, it includes a pair of 2-DOF radial magnetic bearings (2-DOF RMB_{-UP}, 2-DOF RMB_{-LO}) and a pair of 1-DOF axial magnetic bearings (1-DOF RMB_{-UP}, 1-DOF RMB_{-LO}). The arrangement and structure of 2nd type MSFW and the generation of additional tilting torque are shown in Fig. 3, it includes one 2-DOF RAM and a pair of 3-DOF axial magnetic bearings (3-DOF AMB_{-UP}, 3-DOF AMB_{-LO}). The photos of 2-DOF RMB, 1-DOF AMB and 3-DOF AMB are shown in Fig. 4, respectively. All of the 2-DOF RMB, 1-DOF AMB and 3-DOF AMB are permanent magnet biased magnetic bearing, having positive displacement stiffness is one of their intrinsic characteristics.

For the 1st type MSFW shown in Fig. 2, setting J_p, J_e and Ω as the polar inertial moment, equatorial inertial

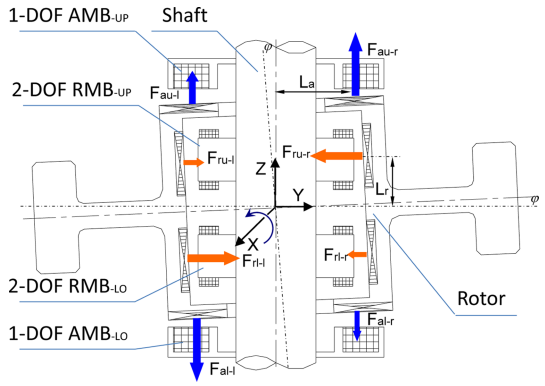

Fig. 2. (Color online) MSFW with 2-DOF RMBs and 1-DOF AMBs.

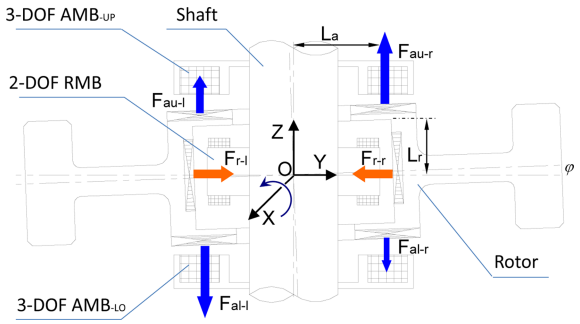

Fig. 3. (Color online) MSFW with 2-DOF RAM and 3-DOF AMBs.

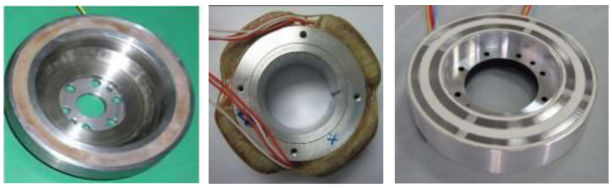

(a) (b) (c)

Fig. 4. (Color online) Different magnetic bearings (a) 1-DOF AMB (b) 2-DOF RMB (c) 3-DOF AMB.

moment and the rotational speed of rotor, respectively. If the rotor was tilted around x-axis (or y-axis) anticlockwise about angle φ per unit time by this pair of 2-DOF RMBs to generate the required gyroscope momentum M_{req}, then

$$M_{req} = J_p \Omega \times \dot{\varphi} \tag{1}$$

The generation of additional tilting torque is also shown in Fig. 2, where L_r presents the distance between the center of 2-DOF RMB$_{-UP}$ or 2-DOF RMB$_{-LO}$ and y-axis, $F_{ru\text{-}l}$ and $F_{ru\text{-}r}$ denote the left suction force and right suction force of 2-DOF RMB$_{-UP}$, respectively, their unbalanced force is $F_{ru\text{-}r} - F_{ru\text{-}l}$. In the same manner, we denote $F_{rl\text{-}l}$ and $F_{rl\text{-}r}$ as the left suction force and right suction force of 2-DOF RMB$_{-LO}$, their unbalanced force is $F_{rl\text{-}l} - F_{rl\text{-}r}$, then the required driving momentum M_d is

$$M_d = J_e \cdot \dot{\varphi} = (F_{ru\text{-}r} - F_{ru\text{-}l} + F_{rl\text{-}l} - F_{rl\text{-}r}) \cdot L_r \tag{2}$$

Then Eq. (1) becomes

$$M_{req} = J_p \Omega \times [(F_{ru\text{-}r} - F_{ru\text{-}l} + F_{rl\text{-}l} - F_{rl\text{-}r})/J_e \cdot L_r] \tag{3}$$

But due to the tilting angle, $F_{au\text{-}r}$ of 1-DOF AMB$_{-UP}$ becomes larger than $F_{au\text{-}l}$, and the $F_{al\text{-}l}$ of 1-DOF AMB$_{-LO}$ becomes larger than $F_{al\text{-}r}$, then the additional torque M_a acting on the rotor produced by 1-DOF AMBs is

$$M_a = (F_{au\text{-}r} - F_{au\text{-}l} + F_{al\text{-}l} - F_{al\text{-}r}) \cdot L_a \tag{4}$$

where L_a presents the distance between the force center of 1-DOF AMB$_{-UP}$ or 1-DOF AMB$_{-LO}$ and z-axis.

So the actual outputting gyroscope momentum M_{act} is

$$M_{act} = J_p \Omega \times [(F_{ru\text{-}r} - F_{ru\text{-}l} + F_{rl\text{-}l} - F_{rl\text{-}r}) \cdot L_r + (F_{au\text{-}r} - F_{au\text{-}l} + F_{al\text{-}l} - F_{al\text{-}r}) \cdot L_a]/J_e \tag{5}$$

The error between M_{req} and M_{act} is $J_p[(F_{au\text{-}r} - F_{au\text{-}l} + F_{al\text{-}l} - F_{al\text{-}r})\cdot L_a]/J_e$, which is difficult to be measured or be compensated effectively, so the attitude of the spacecraft can not be controlled accurately. Similarly, if the rotor was tilted around x-axis (or y-axis) anticlockwise about angle φ per unit time by outer torque to generate the required gyroscope momentum, the error between M_{req} and M_{act} is $J_p[(F_{ru\text{-}r} - F_{ru\text{-}l} + F_{rl\text{-}l} - F_{rl\text{-}r})\cdot L_r + (F_{au\text{-}r} - F_{au\text{-}l} + F_{al\text{-}l} - F_{al\text{-}r})\cdot L_a]/J_e$, which is larger than that produced by a pair of 2-DOF RMBs.

For the 2nd type MSFW shown in Fig. 3, setting the distance between the force center of 3-DOF AMB$_{-UP}$ or 3-DOF AMB$_{-LO}$ and z-axis as L_a, when the rotor is tilted around x- axis (or y-axis) anticlockwise about angle φ per unit time by the pair of 3-DOF AMBs to generate M_{req}, the M_d provided not only by left suction force $F_{au\text{-}l}$ and right suction force $F_{au\text{-}r}$ of 3-DOF AMB$_{-UP}$ but also by left suction force $F_{al\text{-}l}$ and right suction force $F_{al\text{-}r}$ of 3-DOF AMB$_{-LO}$ is

$$M_d = J_e \cdot \dot{\varphi} = (F_{au\text{-}r} - F_{au\text{-}l} + F_{al\text{-}l} - F_{al\text{-}r}) \cdot L_a \tag{6}$$

For the 2-DOF RMB in this MSFW, $F_{r\text{-}l}$ equals $F_{r\text{-}r}$, and both of them across through the centroid of rotor O, then the torque made by them is zero and M_{act} of the rotor is not affected. But the tilting angle of rotor is very small and can't beyond 0.1° generally because the air gap of both 2-DOF RAM and 3-DOF AMB are about 0.3 mm, which is too small for the rotor to tilt about a large angle.

If the rotor is tilted around x-axis (or y-axis) anticlockwise about angle φ per unit time by outer torque to generate the required gyroscope momentum, the torque presented by Eq. (6) becomes the additional torque acting on the rotor, so the error between M_{req} and M_{act} is $J_p[(F_{au\text{-}r} - F_{au\text{-}l} + F_{al\text{-}l} - F_{al\text{-}r})\cdot L_a]/J_e$, which is also difficult to be measured or be compensated effectively, so the attitude of the spacecraft can't be controlled accurately either.

However, no matter what additional torque is, the additional torque acting on the rotor is equal to the product of the unbalanced force and torque arm of the bearing. Even if the positive displacement stiffness is the intrinsic characteristic of AMB or RMB and it is difficult to reduce these unbalanced forces when the rotor tilts, but it is preferable to reduce the torque arm of AMB or RMB by the presented novel RFMB to make the additional torque be zero approximately.

3. Novel RFMB for Gimballing Ability

K. Yabuuchi [15], H. Sawada [12] and Y. Horiuchi [20] presented a conical pure active reluctance force-type magnetic bearing for the attitude control of satellite, but the air gaps of this magnetic bearings are larger than those in common magnetic bearings to enlarge the tilt angle of the flywheel rotor, so they will consume plenty of power on the earth. The force generated by conical stator has component forces in both radial and axial directions, it is crucial to solve the problem of force decoupling to make its control be easier. When the rotor tilts, the air gap is not uniform any more, the flux in one channel (X channel, for

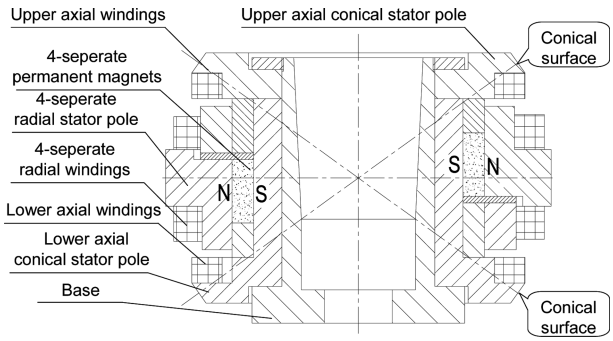

Fig. 5. Schematic diagram of novel RFMB.

example) will leak into adjacent channel (Y channel), what will make the coupling between different channels be more serious. John Watkins [21] proposed a structure with pole-piece separated into two parts tapering mirror images of one another to decouple radial and axial forces, but this structure will result in large additional tilting torque when it is used in the gimballing MSFW.

As shown in Fig. 5, the radial magnetic bearing unit and axial magnetic bearing unit of the presented novel RFMB are integrated as a hybrid reluctance force-type magnetic bearing assembly to ensure the rotor be suspended stably in the central position, permanent magnets are used to generate the radial and axial bias fluxes to suspend the rotor without lots of power consumption when MSFW is on the earth. The radial stators located in the center of RFMB include 4 stator poles, their relative permanent magnets are also separated into four separate segments by nonmagnetic materials. Two stator poles in the same channel are connected by the stator yoke to be a stator subassembly in X or Y channels. Two radial stator subassemblies for X and Y channels are connected perpendicularly with nonmagnetic material, the magnetic flux of X and Y channels are independent from each other. There are two axial conical stators used to control the translation of rotor in Z direction only. One is located at the upper end and another is located at the lower end, and each axial conical stator has one control winding. Because these two conical working air gaps formed between the stator and rotor can make the normal direction of the midst conical faces direct to the centroid of the rotor, so the torque arm of the bearing is approximately zero and its additional torque is also approximately zero consequently when the rotor is tilted.

Generally, the rotor of MSFW is suspended in the central position by the novel RFMB. When the rotor is disturbed to move to Z+ direction, the upper conical air gap would become larger while the lower conical air gap would get smaller along Z direction, so the magnetic flux density and force would get even smaller at the upper conical stator, and the rotor would subject to an additional force in Z+ direction. The integrated axial/radial displacement sensor can detect this axial translation of rotor and transmit the related signals to the control system to prevent the rotor from translating further in Z+ direction. By adding control current through these axial windings, a suitable corrective control flux is generated. The flux paths in X direction are shown in Fig. 6(a), where the biased fluxes generated by permanent magnets are denoted by the solid lines and the control flux generated by windings are denoted by dash line. The biased flux generated from the permanent magnet, which is radically magnetized, is divided into two parts after passing through the radial air gaps: one is the biased flux flowing across the radial stator pole, air gap, the rotor, upper axial air gap and its upper axial stator, and the other is a flux flowing across the radial stator pole, the air gap, the rotor, the lower axial air gap and its lower axial stator. The control flux generated by the current in axial controlling windings flows across the upper stator pole, the upper axial air gap, the rotor, the lower axial air gap and the lower stator pole. By adding the biased flux at the large air gap side and subtracting the biased flux at the small air gap side, then the bearing can produce a restoring force along the axial direction. When the rotor moves in X+ direction or Y direction, the magnetic flux density and force under the X+ radial stator pole decrease while that under the X– radial stator pole increase, so an additional force generates in X+ direction. Due to the conical stators in axial magnetic bearing, their magnetic flux density and force would also decrease under the X+ part. Since the component forces in Z direction generated by the upper and lower conical stators can be counteracted with each other, the component force in X direction is only left. The integrated axial/radial displacement sensor can also detect this state and transmit related signals to the control system to prevent the rotor from translating further in X+ direction. The control flux

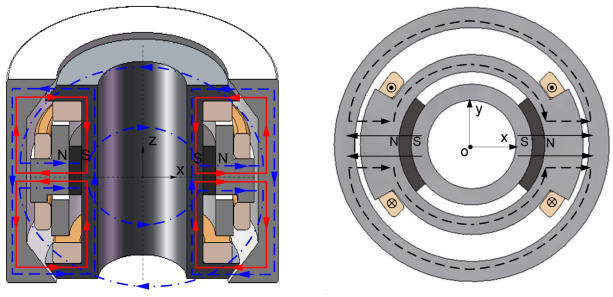

(a) (b)

Fig. 6. (Color online) Novel RFMB (a) flux paths in X direction (b) paths of radial flux in X direction.

generated by the control current in radial windings in X channel is represented by dash line in Fig. 6(b), it flows through the X+ radial air gap, the X channel stator yoke and the X– radial air gap, then the bias flux in the X+ direction is enhanced and the bias fluxes in the X– direction is decreased, therefore, a restoring force is produced and the rotor is moved back toward the central position.

We define F_{pm} and R_{pm} as the magnetic motive force and reluctance of each permanent magnet (A), δ_x, δ_y and δ_z as the displacement in X, Y and Z directions (m), R_{x+} and R_{x-} as reluctances of radial air gap in X+ direction or in X- direction, R_{y+} and R_{y-} as reluctances of radial air gap in Y+ and Y- direction for the radial magnetic bearing unit (1/H), respectively. Define R_{z+} and R_{z-} as reluctances of air gap in Z+ and Z- direction for axial magnetic bearing unit (1/H), respectively. At the same time, the control currents in X direction, Y direction for radial windings and that for axial windings are presented by I_x, I_z, and I_z(A), their relative magnetic motive forces of each control winding are presented by F_{cx} (A), F_{cy} (A) and F_{cz} (A), respectively. $F_{cx} = N_r I_x$, $F_{cy} = N_r I_y$ and $F_{cz} = N_a I_z$, where N_r or N_a is the turn number of the radial or axial

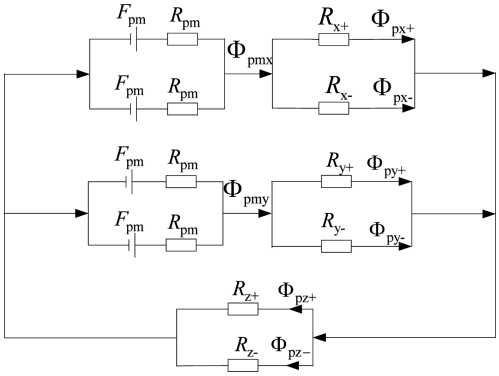

Fig. 7. Equivalent magnetic circuits of permanent magnets.

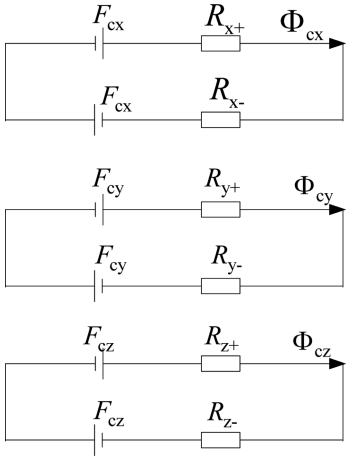

Fig. 8. Equivalent magnetic circuits of control current.

control windings.

Considering the influence of the leakage flux, the equivalent magnetic circuits of permanent magnets in this novel RFMB are simplified as shown in Fig. 7, and its equivalent magnetic circuits of control current are simplified as shown in Fig. 8. We can find out that not only the magnetic flux of the radial magnetic bearing unit in X and Y channels are independent from each other, but also the magnetic fluxes of these conical stators have no effect on that of the radial magnetic bearing unit. Even if the air gap becomes uniform badly when the flywheel rotor tilts, there are not any couple between X and Y channels in the radial magnetic bearing unit or between radial magnetic bearing unit and axial magnetic bearing unit at all. Both the biased fluxes and control fluxes of each air gap are calculated out according to the Ohm's Law of magnetic circuit.

$$\begin{bmatrix} \Phi_{px+} \\ \Phi_{px-} \\ \Phi_{py+} \\ \Phi_{py-} \\ \Phi_{pz+} \\ \Phi_{pz-} \end{bmatrix} = \begin{bmatrix} R_x/R_{x+} & 0 \\ R_x/R_{x-} & 0 \\ 0 & R_y/R_{y+} \\ 0 & R_y/R_{y-} \\ R_z/R_{z+} & R_z/R_{z+} \\ R_z/R_{z-} & R_z/R_{z-} \end{bmatrix} \cdot \begin{bmatrix} \dfrac{2F_{pm}}{\sigma_p\left(R_{pm}+R_x+R_z\right)} \\ \dfrac{2F_{pm}}{\sigma_p\left(R_{pm}+R_y+R_z\right)} \end{bmatrix} \tag{7}$$

where σ_p is the leakage coefficient of the biased flux, σ_r and σ_z are the leakage coefficients of the radial and axial control fluxes, respectively. $R_x = 1/(1/R_{x+} + 1/R_{x-})$, $R_y = 1/(1/R_{y+} + 1/R_{y-})$ and $R_z = 1/(1/R_{z+} + 1/R_{z-})$.

The control flux in each channel can be expressed as

$$\begin{cases} \Phi_{cx} = 2F_{cx}/[(R_{x+}+R_{x-})\cdot\sigma_r] \\ \Phi_{cy} = 2F_{cy}/[(R_{y+}+R_{y-})\cdot\sigma_r] \\ \Phi_{cz} = 2F_{cz}/[(R_{z+}+R_{z-})\cdot\sigma_z] \end{cases} \tag{8}$$

Hence the total flux of each air gap can be expressed as

$$\begin{cases} \Phi_{x+} = \Phi_{px+} + \Phi_{cx}, \quad \Phi_{x-} = \Phi_{px-} - \Phi_{cx} \\ \Phi_{y+} = \Phi_{py+} + \Phi_{cy}, \quad \Phi_{y-} = \Phi_{py-} - \Phi_{cy} \\ \Phi_{z+} = \Phi_{pz+} + \Phi_{cz}, \quad \Phi_{z-} = \Phi_{pz-} - \Phi_{cz} \end{cases} \tag{9}$$

where Φ_{x+} and Φ_{x-} are the total flux of bias and control fluxes in X+ direction and X- direction, Φ_{y+} and Φ_{y-} are the total fluxes in Y+ and Y- directions, Φ_{z+} and Φ_{z-} are the total fluxes in Z+ and Z- directions, respectively.

4. Suspension Properties of Novel RFMB

4.1. Non-coupling suspension forces

By the principle of virtual work, the component force

F_{rx} in X direction and F_{ry} in Y direction of the resultant forces generated by the radial stators are integrated as

$$F_{rx} = \int_{\alpha_{11}}^{\alpha_{12}} \frac{\mu_0 r_s h_{rs} \left(\Phi_{x+} R_{x+}\right)^2 \cdot \cos\theta}{2\delta_g^2 \left(\delta_r, \gamma, \theta\right)} d\theta + \int_{\alpha_{21}}^{\alpha_{22}} \frac{\mu_0 r_s h_{rs} \left(\Phi_{x-} R_{x-}\right)^2 \cdot \cos\theta}{2\delta_g^2 \left(\delta_r, \gamma, \theta\right)} d\theta \quad (10)$$

$$F_{ry} = \int_{\alpha_{31}}^{\alpha_{32}} \frac{\mu_0 r_s h_{rs} \left(\Phi_{y+} R_{y+}\right)^2 \cdot \sin\theta}{2\delta_g^2 \left(\rho_r, \gamma, \theta\right)} d\theta + \int_{\alpha_{41}}^{\alpha_{42}} \frac{\mu_0 r_s h_{rs} \left(\Phi_{y-} R_{y-}\right)^2 \cdot \sin\theta}{2\delta_g^2 \left(\rho_r, \gamma, \theta\right)} d\theta \quad (11)$$

where α_{11}, α_{21}, α_{31} and α_{41} are the starting angles, α_{12}, α_{22}, α_{32} and α_{42} are the ending angles of the four radial stator poles, r_s is the outer radius of the stator, h_{rs} is the height of radial stator iron, δ_g is the length of the radial air gaps and is variable with the angle θ around the circumference. δ_r is the displacement of rotor in radial direction, and $\delta_r = \sqrt{\delta_x^2 + \delta_y^2}$, γ is the direction angle of the rotor displacement vector, and $\gamma = \arctan(\delta_x/\delta_y)$.

As for the force generated by axial conical stator, it includes not only the component force F_{az} in Z direction but also component force F_{ax} and F_{ay} in X and Y directions.

$$F_{ax} = \int_0^{2\pi} \int_0^L \frac{\mu_0 \left(r_c - l\cot\varphi\right)\left(\Phi_{au} R_{au}\right)^2 \cdot \cos\theta}{2\delta_{au}^2 \left(\rho_r, \gamma, \theta, z\right)} dl d\theta + \int_0^{2\pi} \int_0^L \frac{\mu_0 \left(r_c - l\cot\varphi\right)\left(\Phi_{al} R_{al}\right)^2 \cdot \cos\theta}{2\delta_{al}^2 \left(\rho_r, \gamma, \theta, z\right)} dl d\theta \quad (12)$$

$$F_{ay} = \int_0^{2\pi} \int_0^L \frac{\mu_0 \left(r_c - l\cot\varphi\right)\left(\Phi_{au} R_{au}\right)^2 \cdot \sin\theta}{2\delta_{au}^2 \left(\rho_r, \gamma, \theta, z\right)} dl d\theta + \int_0^{2\pi} \int_0^L \frac{\mu_0 \left(r_c - l\cot\varphi\right)\left(\Phi_{al} R_{al}\right)^2 \cdot \sin\theta}{2\delta_{al}^2 \left(\rho_r, \gamma, \theta, z\right)} dl d\theta \quad (13)$$

$$F_{az} = \int_0^{2\pi} \int_0^L \frac{\mu_0 \left(r_c - l\cot\varphi\right)\left(\Phi_{au} R_{au}\right)^2 \cdot \cos\varphi}{2\delta_{au}^2 \left(\rho_r, \gamma, \theta, z\right) \cdot \sin\varphi} dl d\theta - \int_0^{2\pi} \int_0^L \frac{\mu_0 \left(r_c - l\cot\varphi\right)\left(\Phi_{al} R_{al}\right)^2 \cdot \cos\varphi}{2\delta_{al}^2 \left(\rho_r, \gamma, \theta, z\right) \sin\varphi} dl d\theta \quad (14)$$

where r_c the maximum outer radius of the axial conical stator, L is the axial length of the conical stator iron. δ_{au} and δ_{al} are the length of the upper and lower conical air gaps, respectively, both of them vary with the rotor displacement.

The resultant forces generated by both the radial and the conical stators in X, Y and Z direction can be expressed as

$$\begin{cases} F_x = F_{rx} + F_{ax} \\ F_y = F_{ry} + F_{ay} \\ F_z = F_{az} \end{cases} \quad (15)$$

Based on the above equations and parameters of the novel RFMB listed in Table 1, the obtained force-displacement and force-current characteristics are shown

Table 1. Main parameters of the RFMB.

Symbol	Quantity	Designed values
ρ_{c0}	Length of conical gap	0.8 mm
ρ_{r0}	Length of radial gap	0.5 mm
Ds_{ro}	Outer diameter of radial stator	116 mm
Ds_{co}	Maximum outer diameter of conical stator	102 mm
Ls_{ra}	Height of radial stator iron	17 mm
Ls_{ax}	Height of conical stator	6.5 mm
H_c	Coercive force of permanent magnet	760 kA/m
B_r	Remanence of permanent magnet	1.05 T
N_r	Turns of radial control windings	220
N_a	Turns of axial control windings	180
σ_p	Leakage coefficient of bias flux	1.45
σ_r	Leakage coefficient of radial control flux	1.25
σ_a	Leakage coefficient of axial control flux	1.2

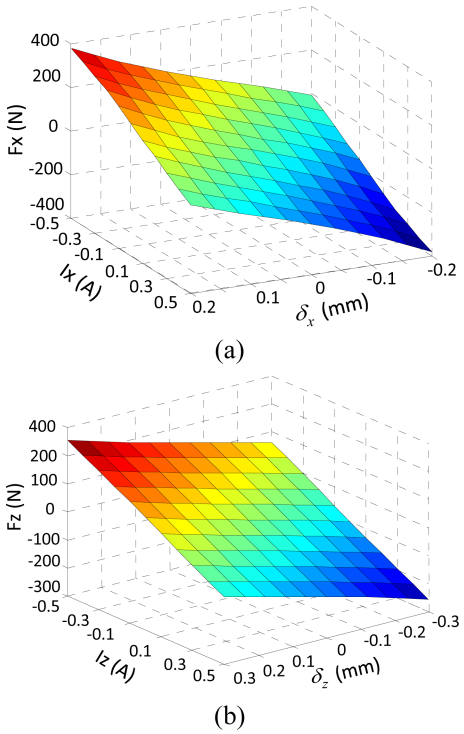

Fig. 9. (Color online) Suspension force (a) F_x versus δ_x and I_x (b) F_z versus δ_z and I_z.

in Fig. 9.

We can find out that both the radial magnetic force and the axial magnetic force are nearly proportional to the displacement of rotor and their relative control current. We also calculated out that the force-displacement stiffness and force-current stiffness of radial magnetic bearing unit are 0.65 N/μm and −380 N/A, and the force-displacement stiffness and force-current stiffness of axial magnetic bearing unit are 0.34 N/μm and −318 N/A, respectively.

In order to analyze the magnetic coupling among X, Y and Z directions, the changes of magnetic forces with variation of current and displacement are analyzed when the rotor is drifted or tilted. Because of the symmetry of the RFMB structure, not all the force coupling analyses in every direction are presented here. For example, when the rotor is drifted a certain displacement (δ_x) in X direction and its corresponding control current I_x is given in these windings in this direction, the force in Y direction can be obtained in case that the offset δ_x = 0.1 mm and the current $I_y = 0$, the coupling analysis between X and Y channels are illustrated in Fig. 10. We can find out that the offset and control current in windings in one direction have little influence on the force in other directions. When the displacement in X direction reaches 0.25 mm, which is the length of protection air gap, the variation of force in Y direction is only 1.6% and the variation of force in Z direction is 2.5%, which can be calculated from Fig. 10(a) and (b). When the position of the rotor is fixed, the forces in Y and Z directions remain unchanged no matter how large the current in X direction is. The force in X direction varies a little with the current and dis-

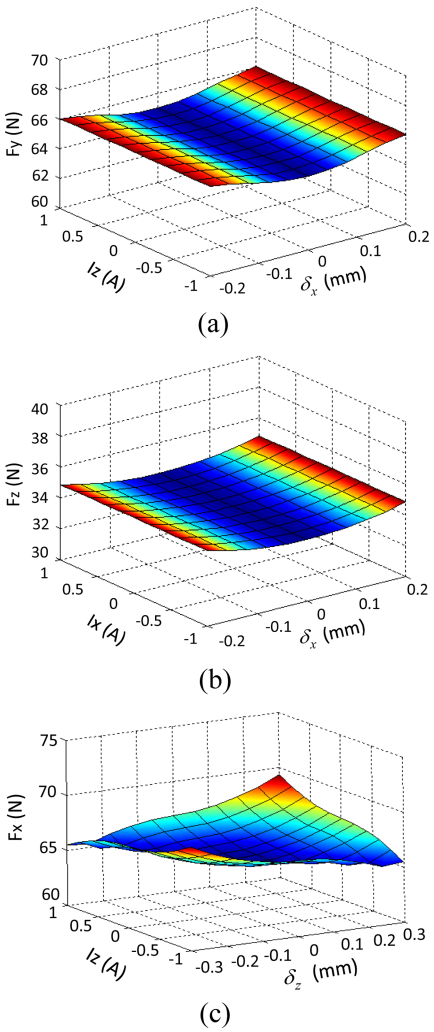

Fig. 10. (Color online) Force coupling with current and displacement (a) F_y versus I_x and δ_x, (b) F_z versus I_x and δ_x, (c) F_x versus I_z and δ_z.

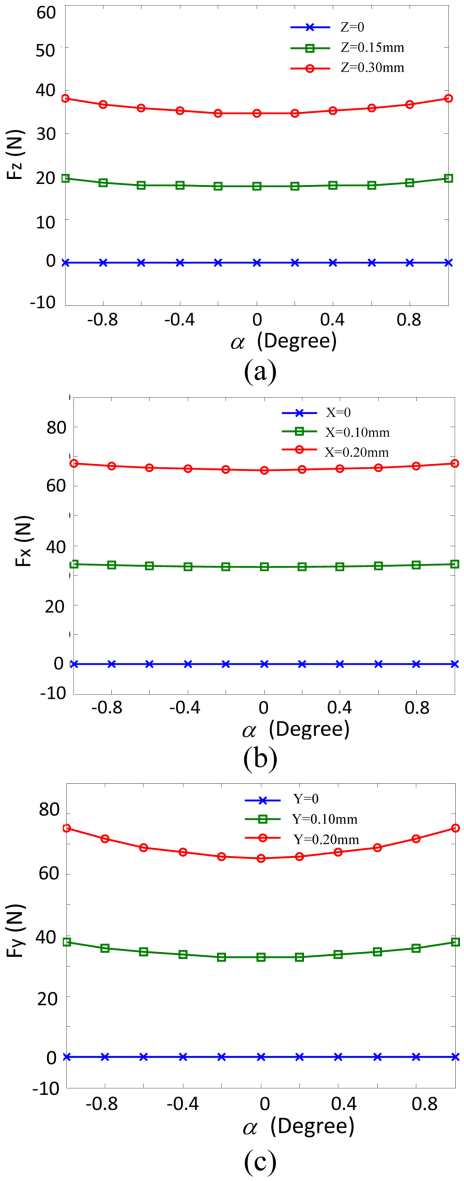

Fig. 11. (Color online) Force coupling with tilting angle. (a) F_z versus α, (b) F_x versus α, (c) F_y versus α.

placement in Z direction due to the radial component force generated by the conical stator, and its maximum variation is not better than 6%. Therefore, magnetic fluxes of the novel RFMB are almost decoupled among different directions when the rotor shifts in some direction.

When the rotor tilts around x or y-axis, the force coupling is also analyzed in case that the rotor drifts a certain displacement in one direction, i.e. X, Y or Z direction. These main analysis results are illustrated in Fig. 11 to express the relationships between F_z and α, F_x and α, F_y and α, respectively.

We can find out that when the centroid of the rotor coincides with that of the novel RFMB, i.e. the rotor does not drift in any direction (x, y, or z direction), the rotor tilting has no influence on its relative force. But when the rotor drifts in some direction, the force in this direction will increase with the increasing of the tilting angle whether the tilting angle is positive or negative. When the rotor tilts around x-axis up to the designed maximum angle 1°, the force change in Z direction is 9% in case of a axial displacement 0.3 mm while the force change will reach 3% in X directions or 14% in Y directions in case of a radial displacement 0.2 mm, respectively. Therefore, the rotor should be suspended well in the central position before the rotor is tilted to generate the required control moment.

4.2. Low additional tilting torque

When the rotor tilts around x or y-axis, the additional tilting torque is caused mainly by the conical stators, especially when the normal direction of the conical faces departs from the center of the rotor. Assuming the rotor tilts around x and y-axis by the angle of α and β, respectively, the torque can be derived as

$$M_x = \int_0^{2\pi}\int_0^L \frac{\mu_0 (r_c - l\cot\varphi)(\phi_{au}R_{au})^2}{2\delta_{au}^2(\theta,\alpha,\beta)\sin\varphi}\cdot l_x(\theta,l)d\theta dl - \int_0^{2\pi}\int_0^L \frac{\mu_0 (r_c - l\cot\varphi)(\phi_{au}R_{au})^2}{2\delta_{al}^2(\theta,\alpha,\beta)\sin\varphi}\cdot l_x(\theta,l)d\theta dl \quad (16)$$

$$M_y = \int_0^{2\pi}\int_0^L \frac{\mu_0 (r_c - l\cot\varphi)(\Phi_{au}R_{au})^2}{2\delta_{au}^2(\theta,\alpha,\beta)\sin\varphi}\cdot l_y(\theta,l)d\theta dl - \int_0^{2\pi}\int_0^L \frac{\mu_0 (r_c - l\cot\varphi)(\Phi_{au}R_{au})^2}{2\delta_{al}^2(\theta,\alpha,\beta)\sin\varphi}\cdot l_y(\theta,l)d\theta dl \quad (17)$$

where,

$$l_x(\theta,l) = (L_p + l)\sin\varphi\cdot\sin\theta - (r_c - l\cot\varphi)\cos\varphi\cdot\sin\theta,$$

$$l_y(\theta,l) = (L_p + l)\sin\varphi\cdot\cos\theta - (r_c - l\cot\varphi)\cos\varphi\cdot\cos\theta.$$

When the rotor is tilted around x or y-axis, the additional tilting torque is mainly caused by the unbalanced force and its related torque arm. The unbalanced force is determined by the uniform distribution of the magnetic flux density around the circumference. In case that the rotor tilts around x-axis about 1°, the distribution of magnetic flux density in the radial and axial air gaps derived by the finite element method (FEM) are shown in Fig. 12(a). The corresponding magnetic flux density curves along the path 1 and path 2 are shown in Fig. 12(b). We can find out that when the rotor tilts around x or y-axis, the magnetic flux density of the conical air gap is uniform around the circumference. The fluctuation of magnetic flux density is from 0.272 T to 0.41 T. The variation trend of magnetic flux density in upper and lower conical air gaps is opposite at any circumferential angle. Therefore, the related magnetic force is uniform around the circumference and the forces of upper and lower conical rotors cannot be counteracted at the same circumferential angle. For the conical rotors, only the normal direction of the conical midst faces directs to the centroid of the rotor, so the torque arm still exists and an additional torque around x or y-axis is generated unavoidably. For the conical axial magnetic bearing in this novel

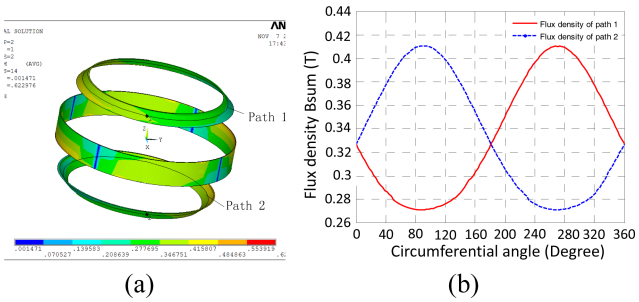

(a) (b)

Fig. 12. (Color online) Magnetic flux density fluctuation in the air gap of RFMB (a) Magnetic field distribution (b) Magnetic flux density curves along path 1 and 2.

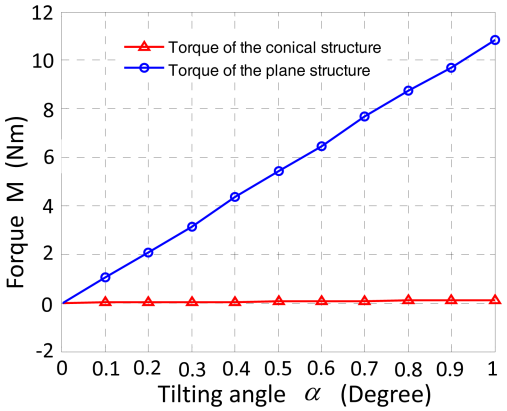

Fig. 13. (Color online) Torque characteristics of magnetic bearing with conical structure or plane structure.

RFMB, the additional torque $M_{a\text{-}r}$ is

$$M_{a\text{-}r} = \int_{S1} \frac{b_1^2(\theta)\cdot l}{2\mu_0} dA + \int_{S2} \frac{b_2^2(\theta)\cdot l}{2\mu_0} dA \quad (18)$$

where $b_1(\theta)$ and $b_2(\theta)$ are the flux densities that vary with the circumferential angle θ, S1 and S2 are the areas of upper and lower conical stators, respectively. l is the normal distance between the vector of the unbalanced force generated by the conical axial magnetic bearing and the centroid of the rotor, it is very small and can be neglected in most cases.

On the other hand, if the rotor of the MSFW with gimballing capability is suspended by the common reluctance force type magnetic bearing as shown in Fig. 3, the generation of additional tilting torque on rotor is same as that shown in Fig. 3. Because the working surface of the 3-DOF MB is plane faces and the torque arm is comparative large, its additional torque is expressed by Eq. (6). Considering the uniform distribution of the magnetic flux density and the additional torque generated by the radial rotors, the relationships between the tilting angle α and the additional tilting torque M of the novel RFMB and that of the common reluctance force-type magnetic bearing with plane faces are analyzed by FEM and these results are illustrated in Fig. 13.

From Fig. 13, we can find out that the additional tilting torques for the presented novel RFMB is 0.05 Nm, which is very small, but the additional tilting torque for the common reluctance force-type magnetic bearing increases with the angle linearly and its maximum torque is up to 11 Nm. We also find out that the angular stiffness calculated from its torque-tilting angle curve for the presented novel RFMB is 0.11 Nm/^{o} while the calculated angular stiffness of the common reluctance force-type magnetic bearing is as much as 10.83 Nm/^{o}. So this novel RFMB will make the MSFW with gimballing capability have high-precision attitude control ability for spacecraft.

5. Eddy Loss of Novel RFMB

In the novel RFMB, these segmented radial stator poles will make the magnetic flux density in the radial rotor be uneven unavoidably, what will result in the enormous eddy loss when the rotor rotates at high speed. The power consumption of the RFMB includes: (1) Copper loss P_{cu} caused by the windings in RFMB, and $P_{cu} = i^2R$, where i is the current in the winding, and R the resistant of the winding, respectively. (2) Iron loss is caused by the magnetic field, which is produced not only by the alternative modulating current in windings but also by the biased permanent magnets. With respect to these materials listed in Table 2, iron loss includes static suspension iron loss and rotational iron loss, and can also be divided into hysteresis loss P_h and eddy loss P_e.

$$P_h = K_h * f_h * B_m^{1.6} V_{fe} \quad (19)$$

$$P_e = K_e \Delta^2 f_h^2 B_m^2 V_{fe} \quad (20)$$

where K_h is the material constant, K_e is coefficient of the material constant, f_h is the alternative frequency of the magnetic field produced by the alternative current, B_m is the magnitude of the changed magnetic flux density for the alternating magnetic field, Δ is the thickness of the material, and V_{fe} is the volume of the iron core for the magnetic pole [19].

For the novel RFMB, there is a biased magnetic field and free of magnetic field alternation between positive and negative, so the hysteresis loss P_h is small enough to be neglected. The eddy loss P_e is the important issue to be focused on. According to Eq. (20), we can reduce the eddy loss of this RFMB by optimization of stator poles to reduce the magnitude of the changed magnetic flux density for the alternating magnetic field and selection of the soft magnetic material with low loss properties such as laminated material, Iron-based Nanocrystalline, amorphous and so on.

5.1. Flux distribution affected by stator poles of RFMB

When the stator pole of this novel RFMB is divided into four segments, a qualitative conclusion can be drawn that the magnetic flux density in the radial rotor plate produced by these poles will change when the rotor rotates. In order to make the difference of the magnetic flux density affected by the permanent magnets and / or the control current in the air gap be smaller, we designed a special structure of the stator pole with shoes for the novel RFMB. So the clearance between poles has been reduced from 30^o to 5^o. With respect to these separate permanent magnets named samarium cobalt permanent magnet with H_{cb} = 760 kA/m and remanence B_r = 1.05T, and the air gap δ = 0.25 mm, the radial distributions of magnetic flux density affected by only the permanent magnets in the air gap of the novel RFMB without/with pole shoes are depicted in Fig. 14 while that affected by both permanent magnets and control current in the air gap of the novel RFMB without/with pole shoes are depicted in Fig. 15, respectively.

From Fig. 14 and Fig. 15, we find out that due to the pole shoes, the areas of the radial poles of this RFMB are enlarged, the maximum magnetic flux density affected by only permanent magnets in the air gap are reduced from 0.47 T to 0.38 T while that affected by permanent magnets

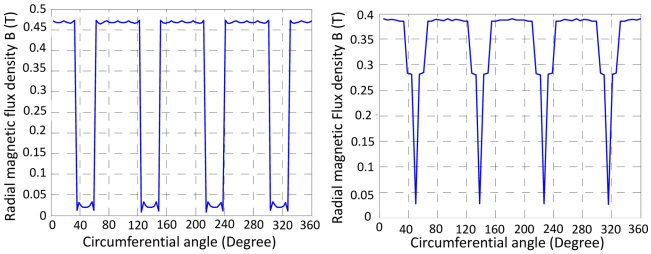

(a) (b)

Fig. 14. (Color online) Radial magnetic flux density affected by permanent magnets in the air gap of RFMB (a) without pole shoes (b) with pole shoes.

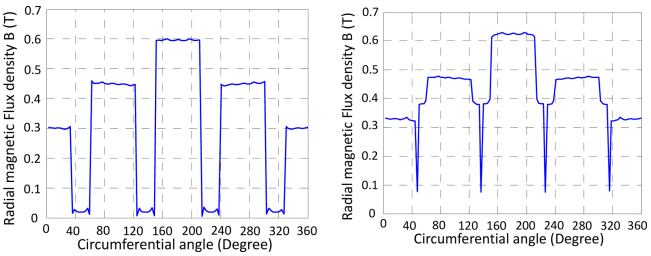

(a) (b)

Fig. 15. (Color online) Radial magnetic flux density affected by permanent magnets and control current 0.1A in the air gap of RFMB (a) without pole shoes (b) with pole shoes.

and control current 0.1 A in the air gap are reduced from 0.6 T to 0.52 T, the variations of magnetic flux density are about 0.08 T, the reduction of the maximum magnetic flux density will reduce the eddy loss of this RFMB effectively. On the other hand, we also find out that due to the pole shoes, the clearance between poles has been reduced from 30° to 5°, the fluctuation of the maximum magnetic flux density affected by only the permanent magnets or both permanent magnets and control current in the air gap still exist, but the duty ratio between the maximum magnetic flux density and minimum magnetic flux density increases greatly, so the eddy loss of the novel RFMB will reduces accordingly.

5.2. Eddy loss affected by different materials of rotor

According to Eq. (20), we can find out that the soft magnetic materials with low loss properties such as laminated material, iron-based nanocrystalline, amorphous and so on will have great effect on the eddy loss of this RFMB. The tested properties of different soft magnetic materials, which are generally used in spacecrafts, are listed in Table 2. Where B_{s1200} present the saturated magnetic flux density (T), H_c presents the coercive force (A/m), B_r the remanence, μ_a initial permeability, μ_m maximum permeability, P_m the iron loss per unit mass when it is subject to the magnetic field either 50 mT with frequency 0.3 kHz or 40 mT with frequency 20 kHz. It is clear that the bulk electro iron DT4 and bulk 1J22 having higher saturated magnetic flux density, but their iron losses per unit mass are the highest among these soft magnetic materials. Although the saturated magnetic flux density of Iron-based Nanocrystalline with 0.03 mm films and Iron-based amorphousness with 0.1 mm films both are comparatively smaller, their iron loss per unit mass are the smallest among these soft magnetic materials, their eddy loss will be smaller when they are used as the rotor for the novel RFMB. Because the Iron-based Nanocrystalline with 0.03 mm films is very crisp and always in reeled state, it is difficult to handle them further, then the Iron-based amorphousness with 0.1 mm films is employed for radial rotor of the novel RFMB.

6. Conclusion

For the gimballing flywheel with existing RFMBs, the additional torques are analyzed considering the positive displacement stiffness of those RFMBs when the rotor tilts. In the novel RFMB, the radial and axial magnetic bearing units are integrated as a compact assembly, permanent magnets are used to generate the radial and axial biased fluxes, the radial stators include 4 stator poles and their relative permanent magnets are also separated into four separate segments to make the magnetic flux in X and Y channels be independent from each other. The radial stator poles are designed four separate poles with shoes and their rotors are made of iron-based amorphous to reduce the eddy loss. Two conical stators are designed

Table 2. Tested properties of different soft magnetic materials.

Items	Bs1200 (T)	Hc (A/m)	Br (T)	μ_a	μ_m	Pm (W/kg) (0.3 kHz, 50 mT)	Pm (W/kg) (20 kHz, 40 mT)
Bulk electro iron DT4	1.8	40	1.6	200	13600	120	280
Bulk 1J22	2.1	170	0.9	800	4500	45	210
Laminated 1J22	2.1	170	0.9	800	4500	8.1	410
Iron-based Nanocrystalline (with 0.03 mm films)	1.2	2	0.4	98000	90000	1.0	36
Iron-based amorphous (with 0.1 mm films)	1.4	28	0.4	1500	30000	4.2	350

to control the translation of rotor in only Z direction without having effects on these forces in radial direction when the rotor tilts around x or y- axis. Simulation results indicated that the fluctuation of magnetic flux density is from 0.272 T to 0.41 T, the additional tilting torques in the novel RFMB is 0.05 Nm while that in the common reluctance force-type magnetic bearing increases with the angle linearly and its maximum torque is up to 11 Nm. When the rotor drifts in some direction, the magnetic fluxes of the novel RFMB are almost decoupled among different directions. When the rotor tilts around x or y-axis, there are 2 conclusions: 1) The rotor tilting has no influence on its relative force if the centroid of the rotor coincides with that of the novel RFMB; 2) The force in this direction will increase with the enlargement of the tilting angle whether the tilting angle is positive or negative when the rotor drifts in some direction, but the maximum changes is not exceed 14%.

Acknowledgment

This work was supported by the National Natural Science Foundation of China under Grant 61174003.

References

[1] B. Penne, C. Tobehn, M. Kassebom, and B. Ziegler, Proceedings of AIAA the 57th International Astronautical Congress, Valencia, Spain (2006).
[2] P. Butz and U. Renner, Proceedings of the 3rd International Symposium on Small Satellites Systems and Services, Annecy, France (1996).
[3] P. Silvestrin, Journal of Annual Review in Control **29**, 247 (2005).
[4] V. Lappas, D. Richie, C. Hall, J. Fausz, and B. Wilson, J. Guid Control Dynam **32**, 354 (2009).
[5] A. Nakajima and C. Murakami, Technical Report of National Aerospace Laboratory, TR-820T (1984).
[6] T. Hashimoto, T. Hamasaki, I. Nakatani, and K. Ninomiya, AIAA-93-3844-CP (1993).
[7] Y.C . Xie, H. Sawada, and T. Hashimoto, Report of Institute of Space and Astronautic Science **680** (2001).
[8] J. G. Bitterly, IEEE Aero. El. Sys. Mag. **13**, 13 (1998).
[9] K. R. Rajagopal and K. K. Sivadasan, J. Appl. Phys. **91**, 6994 (2002).
[10] J. C. Fang and Y. Ren, IEEE Trans. Ind Electron. **58**, 4331 (2011).
[11] B. Gerlach, H. M. Ehinger, and R. Seiler, AIAA Guidance, Navigation, and Control Conference and Exhibit, San Francisco, California, Aug (2005).
[12] H. Sawada, T. Hashimoto, and K. Ninomiya, AIAA Guidance, Navigation, and Control Conference and Exhibit, Denver CO, Aug (2000).
[13] Y. Kim, R. Beach, A. Palazzolo, and A. Provenza, Proceedings of the 1st International Energy Conversion Engineering Conference, Portsmouth, Virginia (2003).
[14] U. Bichler and T. Eckardt, Proceedings of the 1st International Symposium on Magnetic Bearings, Jun. 6-8, ETH Zurich, Switzerland (1988).
[15] K. Yabuuchi, M. Inoue, S. Akishita, *et al*., Proceedings of the 17th Aerospace Mechanisms Symposium, California (1983).
[16] H. Y. Kim and C. W. Lee, Mechatronics **16**, 13 (2006).
[17] J. C. Fang, J. J. Sun, H. Liu, and J. Q. Tang, IEEE Trans. Magn **46**, 4034 (2010).
[18] J. J. Sun, and J. C. Fang, J. Magn. Magn. Mater. **323**, 202 (2011).
[19] J. Q. Tang, J. J. Sun, J. C. Fang, and S. Z. Sam Ge, J. Magn. Magn. Mater. **329**, 153 (2013).
[20] Y. Horiuchi and M. Inoue, Proceedings of the 7th International Symposium on Magnetic Bearings, ETH, Zurich (2000).
[21] J. Watkins, G. Brown, and K. Blumenstock, Proceedings of the 33rd Southeastern Symposium on System Theory, Athens, OH (2001).